# CMS Physics Analysis Summary

Contact: cms-pag-conveners-smp@cern.ch 2015/11/13

# Measurement of inclusive W and Z boson production cross sections in pp collisions at $\sqrt{s} = 13$ TeV

The CMS Collaboration

## Abstract

A measurement of total inclusive and fiducial W and Z boson production cross sections in pp collisions at $\sqrt{s} = 13$ TeV is presented. Electron and muon final states are studied in a data sample collected with the CMS detector corresponding to an integrated luminosity of up to $43 \pm 2\text{pb}^{-1}$. The measured total inclusive cross sections times branching fractions are $\sigma(\text{pp} \to \text{W}^+X) \times \mathcal{B}(\text{W}^+ \to \ell^+\nu)$ = 11370 $\pm$ 50 (stat) $\pm$ 230 (syst) $\pm$ 550 (lumi) pb, $\sigma(\text{pp} \to \text{W}^-X) \times \mathcal{B}(\text{W}^- \to \ell^-\bar{\nu}) = 8580 \pm 50$ (stat) $\pm$ 160 (syst) $\pm$ 410 (lumi) pb, and $\sigma(\text{pp} \to \text{Z}X) \times \mathcal{B}(\text{Z} \to \ell^+\ell^-) = 1910 \pm 10$ (stat) $\pm$ 40 (syst) $\pm$ 90 (lumi) pb for the dilepton mass in the range of 60 to 120 GeV. The measured values agree with next-to-next-to-leading-order QCD cross section calculations. Inclusive cross sections and ratios of cross sections are reported.

# 1 Introduction

The production of W and Z bosons is one of the most prominent examples of hard scattering processes at hadron colliders [1]. Theoretical predictions are available at next-to-next-to-leading order (NNLO) [2–6] in perturbative quantum chromodynamics (QCD). The calculations are limited by uncertainties in parton distribution functions (PDFs), missing higher-order QCD effects, and electroweak (EW) radiative corrections, which are available at next-to-leading order (NLO) [7–10]. Precise measurements of inclusive cross sections provide tests of perturbative QCD and validate the theoretical predictions of higher-order corrections. Additionally, accurate measurements can be used to constrain PDFs.

Inclusive W and Z boson production cross sections, their ratios, and differential cross sections were previously measured by the ATLAS and CMS Collaborations at the CERN large hadron collider (LHC) in proton-proton collisions at $\sqrt{s} = 7$ TeV and 8 TeV [11–13].

This Summary describes the inclusive measurement at $\sqrt{s} = 13$ TeV, performed in the electron and muon decay channels, with the CMS detector. A data sample collected in 2015 corresponding to an integrated luminosity of up to $43 \pm 2\,\text{pb}^{-1}$ is used.

# 2 The CMS experiment

The central feature of the CMS apparatus is a superconducting solenoid, of 6 m internal diameter, providing a field of 3.8 T. Within the field volume are a silicon pixel and strip tracker, a crystal electromagnetic calorimeter (ECAL), and a brass/scintillator hadron calorimeter. Muons are measured in gas-ionization detectors embedded in the steel flux-return yoke of the magnet. CMS uses a right-handed coordinate system, with the origin at the nominal interaction point, the $x$ axis pointing to the center of the LHC, the $y$ axis pointing upwards, perpendicular to the plane of the LHC ring, and the $z$ axis along the counterclockwise-beam direction. The polar angle $\theta$ is measured from the positive $z$ axis, and the azimuthal angle $\phi$ is measured in the $x$-$y$ plane. The pseudorapidity $\eta$ is defined by $\eta = -\ln[\tan(\theta/2)]$. Details of the CMS detector and its performance can be found in Ref. [14].

# 3 Data and simulation events

Because of the high rate of collisions and the limited bandwidth for data processing, the data acquisition system must be selective in deciding which events are sufficiently interesting to be kept for analysis. The trigger makes rapid decisions by executing simplified muon and electron reconstruction algorithms. For this analysis, the events are collected when triggered by the presence of at least one electron with large transverse energy, $E_\text{T} > 23$ GeV, and $|\eta| < 2.5$, or at least one muon with large transverse momentum, $p_\text{T} > 20$ GeV, and $|\eta| < 2.4$, with loose isolation and identification requirements.

Several Monte Carlo event generators are used to simulate the signal and background processes. The MadGraph5_aMC@NLO program [15] provides event samples for the W and Z boson signal and top background, using the NNPDF 3.0 [16] PDF and PYTHIA 8 [17, 18] for the parton shower. Diboson backgrounds are generated using POWHEG [19–22] and PYTHIA 8. For all processes, the detector response is simulated using a detailed description of the CMS detector, based on the GEANT4 package [23]. Minimum bias events are superimposed on the simulated events to emulate the additional pp interactions per bunch crossing (pileup). These samples are reweighted to represent the pileup distribution as measured in the data. The aver-

age number of pileup events per beam crossing in the analyzed data collected in 2015 is about twenty.

## 4 Object and event selection

Leptonic W boson decays are characterized by a prompt, energetic, and isolated charged lepton and a neutrino giving rise to significant missing transverse energy, $E_{\mathrm{T}}^{\mathrm{miss}}$. Events used in the cross section measurement are not required to have a minimum reconstructed $E_{\mathrm{T}}^{\mathrm{miss}}$, but the $E_{\mathrm{T}}^{\mathrm{miss}}$ distribution is used as a discriminant against background from multijet events. The Z boson decays to leptons are selected by requiring two energetic and isolated leptons of the same flavor and, in the case of the muon channel, opposite charge. The Z boson candidates are required to have a reconstructed dilepton mass between 60 and 120 GeV. Samples of Z boson candidates satisfying looser lepton requirements are used to estimate efficiencies. Measurements are performed in the electron and muon decay channels.

Electrons are identified as clusters of energy deposits in the ECAL matched to tracks measured with the silicon tracker [24–28]. The ECAL fiducial region is defined by $|\eta| < 1.444$ (barrel) or $1.566 < |\eta| < 2.5$ (endcap), where $\eta$ is the pseudorapidity of the energy cluster. The barrel-endcap transition region and the first ring of endcap trigger towers are excluded because they are partially obscured by cables and services exiting between the barrel and endcaps. A cluster is considered to be within the acceptance of the ECAL if it is within the ECAL fiducial region and has transverse energy $E_{\mathrm{T}} > 25\,\mathrm{GeV}$. Electrons candidates are identified using the simple cut-based approach using information of the cluster shape, hadronic activity, and track quality. Electrons are required to be isolated from other reconstructed particles in a cone of $\Delta R = 0.3$, where $\Delta R = \sqrt{\Delta\eta^2 + \Delta\phi^2}$. Particle candidates are identified using a particle-flow algorithm [29, 30] that provides a complete description of the event in terms of electrons, muons, photons, charged hadrons, and neutral hadrons. An electron candidate is selected if the sum of transverse momenta of particles in the cone is less than 11% of the candidate's transverse energy.

Muons are reconstructed from seed tracks in the muon detector combined with silicon strip and pixel information using a global fit [31, 32]. In the $p_{\mathrm{T}}$ range of interest, the momentum resolution is driven by the inner tracking system. Muons with $p_{\mathrm{T}} > 25\,\mathrm{GeV}$ and $|\eta| < 2.4$ are selected, which is consistent with the acceptance of the single muon trigger. Muon candidates are identified using the simple cut-based approach using information of the track and global fit quality. A relative isolation variable is computed as discussed for electrons, but in a cone of radius $\Delta R = 0.4$ and with an isolation selection requirement of less than 12%.

## 5 Acceptance and efficiencies

The acceptance for W or Z boson events is the fraction of generated events for which the leptons satisfy the restrictions on $\eta$ and $p_{\mathrm{T}}$. The event selection criteria will select a subset of the accepted events, and the efficiency specifies the fraction of events selected. Explicitly, the electron are required to have $p_T > 25\,\mathrm{GeV}$ and $|\eta| < 1.4442$ or $1.566 < |\eta| < 2.5$, while the muons must have $p_T > 25\,\mathrm{GeV}$ and $|\eta| < 2.4$. For Z boson events, only events generated with $60\,\mathrm{GeV} < m_Z < 120\,\mathrm{GeV}$ are considered. Other detector non-uniformities are accounted for in the efficiency to reconstruct leptons. This acceptance definition is used to separate experimental from theoretical uncertainties in the measurement. Data to simulation ratios of efficiencies are used as scale factors. No single event generator gives a reliable description of both EW

and QCD effects. The acceptance is estimated using Monte Carlo simulation based on MadGraph5_aMC@NLO. The effects of non-perturbative QCD, higher-order QCD, and electroweak corrections on the estimated acceptance are investigated using specific simulation tools, from which uncertainties are derived [7–10, 33, 34]. The experimental results are quoted for NNPDF 3.0. The uncertainty related to the PDF is estimated following the NNPDF prescription.

## 6 Signal extraction

The W boson candidate events are required to have an identified electron or muon. The W boson signal and background yields are obtained from the $E_{\mathrm{T}}^{\mathrm{miss}}$ distributions using a unbinned maximum-likelihood fit. The missing transverse energy is calculated with the particle-flow algorithm by adding the transverse energy vectors of all identified particles. Particle-flow candidates with absolute pseudorapidity larger than 3.0 are not considered in the $E_{\mathrm{T}}^{\mathrm{miss}}$ calculation. These are measured using the forward hadronic calorimeter (HF) which is not fully commissioned for the analyzed data. Based on its properties, each particle is associated with a weight, which describes its probability to originate from pileup and is used to rescale its four-momentum [35]. After rescaling, particles with a very small weight or a very small transverse momentum are discarded. The transverse energy vectors of the pileup corrected particles are then added up to determine $E_{\mathrm{T}}^{\mathrm{miss}}$. Since the missing transverse energy reconstruction algorithm already includes pileup jet removal, no further pileup corrections are applied. An accurate $E_{\mathrm{T}}^{\mathrm{miss}}$ measurement is essential to distinguish the W boson signal from QCD multijet backgrounds. The missing transverse energy response and resolution is derived from a Z boson sample. The recoil in these events is studied in data and the measured performance is applied to the simulation as a function of the $p_{\mathrm{T}}$ of the generated W boson. Other background processes from $\mathrm{W} \to \tau\nu$, Drell–Yan, diboson, and top-pair production also become significant at high $E_{\mathrm{T}}^{\mathrm{miss}}$, contributing about 10% of the total selected yield. The background contribution from cosmic rays in the $\mathrm{W} \to \mu\nu$ channel is negligible. The $E_{\mathrm{T}}^{\mathrm{miss}}$ model is fitted to the observed distribution as the sum of three contributions: the W boson signal, the QCD background, and other backgrounds. The QCD background is modeled by an analytic function, while the signal and EW backgrounds are modeled with simulation-based fitting functions [11]. The EW contributions are normalized to the W boson signal yield in the fit through the ratios of the theoretical cross sections. Figure 1 shows the $E_{\mathrm{T}}^{\mathrm{miss}}$ distributions of the inclusive W boson samples and the results of the fit.

To extract the Z boson yield, the events in the dilepton mass window are counted. The yields contain a contribution of about 3% from $\gamma^*$-mediated processes, including interference effects, as estimated with MCFM [36]. Background contamination is estimated from simulation to be about 0.6%. Figure 2 shows the dilepton mass distributions of the inclusive Z samples. The signal yields, the acceptances, and the efficiencies are summarized in Table 1.

## 7 Systematic uncertainties

The systematic uncertainties are summarized in Table 2 for the electron channel and in Table 3 for the muon channel. The leading experimental uncertainty in the measurement of inclusive cross sections comes from the integrated luminosity of the data sample. The luminosity of the data sample is measured with an uncertainty of 4.8%. Future calibrations of the luminosity, by means of a procedure pioneered by van der Meer [37], consisting of beam scans along the vertical and horizontal directions, will improve this uncertainty significantly and might lead to a shift of the mean value of the inclusive cross sections. In measurements of the ratios of cross

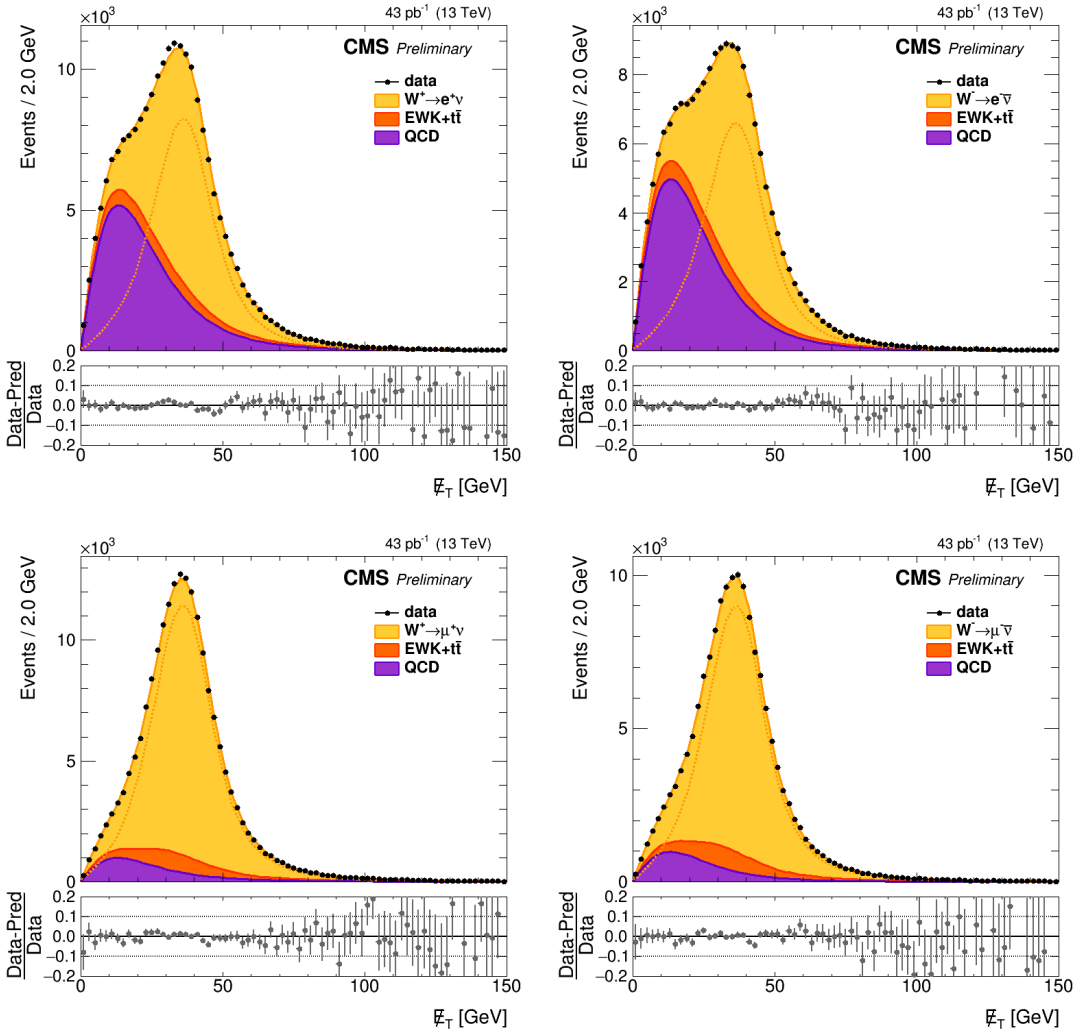


Figure 1: The missing transverse energy distributions for $W^+$ (left) and $W^-$ (right) boson candidate events in the electron (top) and muon (bottom) final states. The dotted orange lines shows the distribution of the W boson signal.

sections this uncertainty cancels. The second leading experimental uncertainty comes from the measurement of the lepton reconstruction and identification efficiency, which is larger in the electron channel. Other uncertainties come from theoretical uncertainties, which are dominated by the resummation and initial state radiation uncertainties. For the measurement of the ratios of cross sections the correlations for the theoretical uncertainties are taken into account.

The systematic uncertainties affecting the shape of the $E_{\mathrm{T}}^{\mathrm{miss}}$ distribution are considered with alternative shapes in the maximum-likelihood fit. These include uncertainties in modeling the lepton momentum scale and resolution and also in the $E_{\mathrm{T}}^{\mathrm{miss}}$ scale and resolution.

# 8 Results

The theoretical predictions of cross sections and cross section ratios are computed at NNLO with the program FEWZ [38–41] and the NNPDF 3.0 set of PDFs. The uncertainties in these predictions, at the 68% CL, include contributions from the uncertainty of the strong coupling constant $\alpha_s$ [42, 43], the choice of heavy-quark masses (charm and bottom quarks) [44], as well as

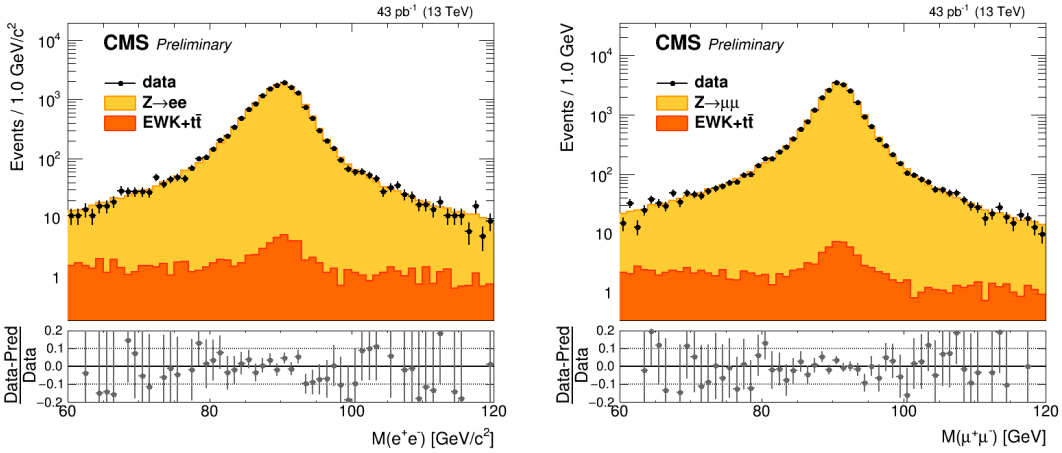


Figure 2: The dilepton mass distributions for Z boson candidate events in the electron (left) and muon (right) final states.

Table 1: The background subtracted signal yields, acceptances, and efficiencies. The Z boson yield uncertainties are given by Poisson statistics, while the W boson yield uncertainties are determined from the fit. Uncertainties in the acceptances and efficiencies are discussed in Section 7.

| Source | $Z \to e^+e^-$ | $W^+ \to e^+\nu$ | $W^- \to e^-\overline{\nu}$ |
|---|---|---|---|
| Yields | $15290 \pm 120$ | $122320 \pm 980$ | $98200 \pm 950$ |
| Acceptance | $0.33 \pm 0.01$ | $0.43 \pm 0.01$ | $0.44 \pm 0.01$ |
| Efficiency | $0.56 \pm 0.04$ | $0.58 \pm 0.02$ | $0.60 \pm 0.02$ |
| Source | $Z \to \mu^+\mu^-$ | $W^+ \to \mu^+\nu$ | $W^- \to \mu^-\overline{\nu}$ |
| Yields | $23670 \pm 150$ | $167710 \pm 830$ | $131250 \pm 910$ |
| Acceptance | $0.36 \pm 0.01$ | $0.44 \pm 0.01$ | $0.46 \pm 0.01$ |
| Efficiency | $0.80 \pm 0.02$ | $0.78 \pm 0.01$ | $0.79 \pm 0.01$ |

Table 2: Systematic uncertainties in percent for the electron channel. "NA" means that the source either does not apply or is negligible.

| Source | $W^+$ | $W^-$ | $W$ | $W^+/W^-$ | $Z$ | $W^+/Z$ | $W^-/Z$ | $W/Z$ |
|---|---|---|---|---|---|---|---|---|
| Lepton charge, reco. & id. [%] | 2.1 | 2.0 | 2.1 | 0.6 | 2.5 | 1.2 | 1.0 | 1.0 |
| Bkg. subtraction / modeling [%] | 1.4 | 1.4 | 1.4 | 0.9 | 0.6 | 1.5 | 1.5 | 1.5 |
| $E_T^{miss}$ scale and resolution | | | shape | | NA | | shape | |
| Electron scale and resolution | | | shape | | NA | | shape | |
| Total experimental [%] | 2.5 | 2.5 | 2.5 | 1.1 | 2.6 | 1.9 | 1.8 | 1.8 |
| Theoretical uncertainty [%] | 1.6 | 1.4 | 1.4 | 1.9 | 1.6 | 1.9 | 1.9 | 1.7 |
| Lumi [%] | 4.8 | 4.8 | 4.8 | NA | 4.8 | NA | NA | NA |
| Total [%] | 5.6 | 5.6 | 5.6 | 2.1 | 5.7 | 2.7 | 2.6 | 2.5 |

Table 3: Systematic uncertainties in percent for the muon channel. "NA" means that the source either does not apply or is negligible.

| Source | $W^+$ | $W^-$ | $W$ | $W^+/W^-$ | $Z$ | $W^+/Z$ | $W^-/Z$ | $W/Z$ |
|---|---|---|---|---|---|---|---|---|
| Lepton charge, reco. & id. [%] | 1.9 | 1.7 | 1.8 | 0.3 | 2.2 | 0.6 | 0.6 | 0.6 |
| Bkg. subtraction / modeling [%] | 0.6 | 0.6 | 0.6 | 0.4 | 0.6 | 0.8 | 0.8 | 0.8 |
| $E_{\mathrm{T}}^{\mathrm{miss}}$ scale and resolution | | | shape | | NA | | shape | |
| Muon scale and resolution | | | shape | | NA | | shape | |
| Total experimental [%] | 2.0 | 1.8 | 1.9 | 0.5 | 2.3 | 1.1 | 1.1 | 1.1 |
| Theoretical Uncertainty [%] | 2.0 | 1.7 | 1.3 | 2.3 | 1.5 | 2.0 | 1.9 | 1.6 |
| Lumi [%] | 4.8 | 4.8 | 4.8 | NA | 4.8 | NA | NA | NA |
| Total [%] | 5.6 | 5.4 | 5.3 | 2.3 | 5.5 | 2.3 | 2.2 | 1.9 |

neglected higher-order corrections beyond NNLO, which are estimated by allowing the renormalization and factorization scales to vary within a factor of two. Both scales are varied up and down together. The NNLO predictions for the total cross sections times branching fractions are $11330 \pm 300$ pb for $W^+$, $8370 \pm 230$ pb for $W^-$, and $1870 \pm 50$ pb for Z boson production. The Z boson cross section requires an invariant mass within the range 60 to 120 GeV, and it includes the effects of virtual photons.

The results are presented as total and fiducial inclusive cross section measurement. For fiducial measurements the systematic uncertainties are reduced because no theoretical extrapolation of the result to the full phase space is performed. The measurements of the W and Z boson cross sections in the electron and muon channel yield a test of lepton universality. The results in the electron and muon decay channels are compatible with a p-value of 0.85. Figure 3 shows the ratios of the total inclusive cross sections compared to previous experimental checks of lepton universality and the standard-model expectation. Assuming universality of lepton couplings to W and Z bosons, the channels are combined by calculating an average cross section value weighted by their statistical and systematic uncertainties. In the combination the luminosity uncertainty is assumed to be fully correlated and the other uncertainties are treated as uncorrelated.

A summary of total and fiducial inclusive $W^+$, $W^-$, W, and Z production cross sections times branching fractions, $W^+$, $W^-$, and W to Z and $W^+$ to $W^-$ ratios, and their theoretical predictions are shown in Table 4 and Table 5. Figure 4 and Figure 5 show the ratio of the experimental results and the theoretical predictions.

The predictions of the total and fiducial inclusive cross sections and their ratios have been calculated for five PDF sets: NNPDF3.0, CT14 [45], MMHT2014 [46], ABM12LHC [47], and HERAPDF15 [48]. As discussed earlier, the theoretical predictions are derived with FEWZ. The uncertainties have contributions from the uncertainty of $\alpha_s$, the choice of heavy-quark masses (charm and bottom quarks), as well as neglected higher-order corrections beyond NNLO, which are estimated by allowing the renormalization and factorization scales to vary within a factor of two. The predictions are summarized in Table 6 and shown in comparison with the measured results for cross sections and ratios of cross sections of the $W^+$ and $W^-$ to Z and $W^+$ to $W^-$ fiducial cross sections in Figure 6 and Figure 7. The predictions agree well with the measurements. The experimental precision is already comparable with theoretical uncertainties. The uncertainty on the preliminary luminosity calibration dominates the comparison.

Figure 8 and Figure 9 show the measured and predicted $W^+$ versus $W^-$ and the W versus Z fiducial cross sections for five different PDF sets.

Figure 10 shows the measurements of the total $W^+$, $W^-$, W, and Z production cross sections

Table 4: Summary of total inclusive $W^+$, $W^-$, W, and Z production cross sections times branching fractions, $W^+$, $W^-$, and W to Z and $W^+$ to $W^-$ ratios, and their theoretical predictions.

| Channel | | $\sigma \times \mathcal{B}$ [pb] (total) | NNLO [pb] |
|---|---|---|---|
| | $e^+\nu$ | $11390 \pm 90\,(\text{stat}) \pm 340\,(\text{syst}) \pm 550\,(\text{lumi})$ | |
| $W^+$ | $\mu^+\nu$ | $11350 \pm 60\,(\text{stat}) \pm 320\,(\text{syst}) \pm 550\,(\text{lumi})$ | $11330^{+320}_{-270}$ |
| | $\ell^+\nu$ | $11370 \pm 50\,(\text{stat}) \pm 230\,(\text{syst}) \pm 550\,(\text{lumi})$ | |
| | $e^-\nu$ | $8680 \pm 80\,(\text{stat}) \pm 250\,(\text{syst}) \pm 420\,(\text{lumi})$ | |
| $W^-$ | $\mu^-\nu$ | $8510 \pm 60\,(\text{stat}) \pm 210\,(\text{syst}) \pm 410\,(\text{lumi})$ | $8370^{+240}_{-210}$ |
| | $\ell^-\nu$ | $8580 \pm 50\,(\text{stat}) \pm 160\,(\text{syst}) \pm 410\,(\text{lumi})$ | |
| | $e\nu$ | $20070 \pm 120\,(\text{stat}) \pm 570\,(\text{syst}) \pm 960\,(\text{lumi})$ | |
| W | $\mu\nu$ | $19870 \pm 80\,(\text{stat}) \pm 460\,(\text{syst}) \pm 950\,(\text{lumi})$ | $19700^{+560}_{-470}$ |
| | $\ell\nu$ | $19950 \pm 70\,(\text{stat}) \pm 360\,(\text{syst}) \pm 960\,(\text{lumi})$ | |
| | $e^+e^-$ | $1920 \pm 20\,(\text{stat}) \pm 60\,(\text{syst}) \pm 90\,(\text{lumi})$ | |
| Z | $\mu^+\mu^-$ | $1900 \pm 10\,(\text{stat}) \pm 50\,(\text{syst}) \pm 90\,(\text{lumi})$ | $1870^{+50}_{-40}$ |
| | $\ell^+\ell^-$ | $1910 \pm 10\,(\text{stat}) \pm 40\,(\text{syst}) \pm 90\,(\text{lumi})$ | |
| Quantity | | Ratio (total) | NNLO |
| | e | $1.313 \pm 0.016\,(\text{stat}) \pm 0.028\,(\text{syst})$ | |
| $R_{W^+/W^-}$ | $\mu$ | $1.334 \pm 0.011\,(\text{stat}) \pm 0.031\,(\text{syst})$ | $1.354^{+0.011}_{-0.012}$ |
| | $\ell$ | $1.323 \pm 0.010\,(\text{stat}) \pm 0.021\,(\text{syst})$ | |
| | e | $5.94 \pm 0.07\,(\text{stat}) \pm 0.16\,(\text{syst})$ | |
| $R_{W^+/Z}$ | $\mu$ | $5.98 \pm 0.05\,(\text{stat}) \pm 0.14\,(\text{syst})$ | $6.06^{+0.04}_{-0.05}$ |
| | $\ell$ | $5.96 \pm 0.04\,(\text{stat}) \pm 0.10\,(\text{syst})$ | |
| | e | $4.52 \pm 0.06\,(\text{stat}) \pm 0.12\,(\text{syst})$ | |
| $R_{W^-/Z}$ | $\mu$ | $4.49 \pm 0.04\,(\text{stat}) \pm 0.10\,(\text{syst})$ | $4.48^{+0.03}_{-0.02}$ |
| | $\ell$ | $4.50 \pm 0.03\,(\text{stat}) \pm 0.08\,(\text{syst})$ | |
| | e | $10.46 \pm 0.11\,(\text{stat}) \pm 0.26\,(\text{syst})$ | |
| $R_{W/Z}$ | $\mu$ | $10.47 \pm 0.08\,(\text{stat}) \pm 0.20\,(\text{syst})$ | $10.55^{+0.07}_{-0.06}$ |
| | $\ell$ | $10.46 \pm 0.06\,(\text{stat}) \pm 0.16\,(\text{syst})$ | |

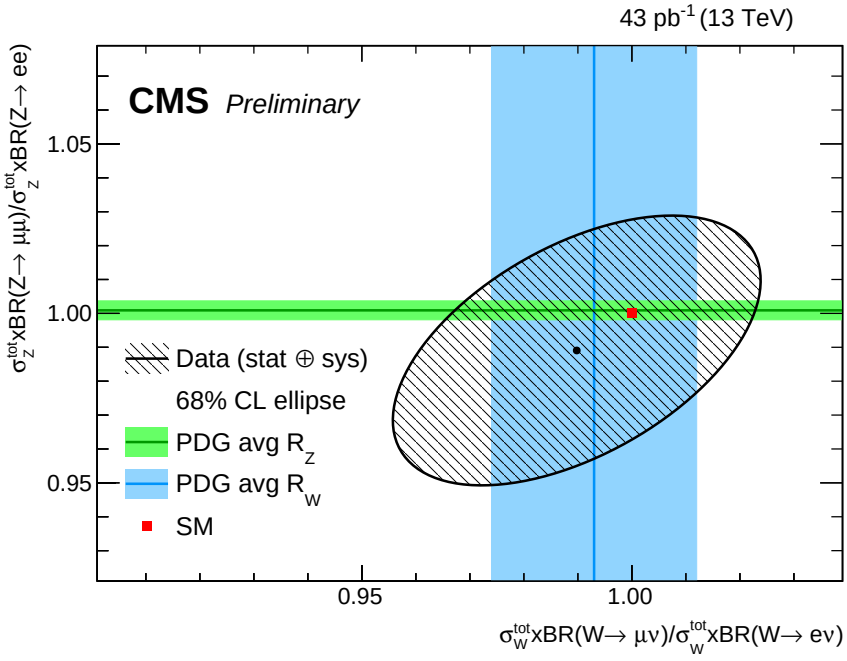


Figure 3: Ratios of the W and Z boson total inclusive cross sections in the electron and muon channels compared to previous experimental checks of lepton universality and the standard-model expectation. The contour obtained from the data (full circle) represent the 68% CL (full line) area accounting for the full set of statistical and systematic uncertainties.

Table 5: Summary of fiducial inclusive $W^+$, $W^-$, W, and Z production cross sections times branching fractions, $W^+$, $W^-$, and W to Z and $W^+$ to $W^-$ ratios, and their theoretical predictions.

| Channel | | $\sigma \times \mathcal{B}$ [pb] (fiducial) | NNLO [pb] |
|---|---|---|---|
| $W^+$ | $e^+\nu$ | $4900 \pm 40\,(\text{stat}) \pm 120\,(\text{syst}) \pm 240\,(\text{lumi})$ | $4870^{+160}_{-140}$ |
| | $\mu^+\nu$ | $5040 \pm 20\,(\text{stat}) \pm 100\,(\text{syst}) \pm 240\,(\text{lumi})$ | $5030^{+180}_{-160}$ |
| $W^-$ | $e^-\nu$ | $3830 \pm 40\,(\text{stat}) \pm 90\,(\text{syst}) \pm 180\,(\text{lumi})$ | $3690^{+150}_{-110}$ |
| | $\mu^-\nu$ | $3900 \pm 30\,(\text{stat}) \pm 70\,(\text{syst}) \pm 190\,(\text{lumi})$ | $3840^{+160}_{-120}$ |
| W | $e\nu$ | $8730 \pm 50\,(\text{stat}) \pm 220\,(\text{syst}) \pm 420\,(\text{lumi})$ | $8570^{+340}_{-240}$ |
| | $\mu\nu$ | $8950 \pm 40\,(\text{stat}) \pm 170\,(\text{syst}) \pm 430\,(\text{lumi})$ | $8870^{+350}_{-240}$ |
| Z | $e^+e^-$ | $640 \pm 10\,(\text{stat}) \pm 20\,(\text{syst}) \pm 30\,(\text{lumi})$ | $620^{+20}_{-20}$ |
| | $\mu^+\mu^-$ | $690 \pm 10\,(\text{stat}) \pm 20\,(\text{syst}) \pm 30\,(\text{lumi})$ | $680^{+30}_{-20}$ |
| Quantity | | Ratio (fiducial) | NNLO |
| $R_{W^+/W^-}$ | e | $1.28 \pm 0.02\,(\text{stat}) \pm 0.01\,(\text{syst})$ | $1.32^{+0.03}_{-0.03}$ |
| | $\mu$ | $1.29 \pm 0.01\,(\text{stat}) \pm 0.01\,(\text{syst})$ | $1.31^{+0.03}_{-0.03}$ |
| $R_{W^+/Z}$ | e | $7.65 \pm 0.09\,(\text{stat}) \pm 0.15\,(\text{syst})$ | $7.82^{+0.17}_{-0.16}$ |
| | $\mu$ | $7.33 \pm 0.06\,(\text{stat}) \pm 0.08\,(\text{syst})$ | $7.43^{+0.17}_{-0.16}$ |
| $R_{W^-/Z}$ | e | $5.97 \pm 0.08\,(\text{stat}) \pm 0.11\,(\text{syst})$ | $5.92^{+0.12}_{-0.11}$ |
| | $\mu$ | $5.67 \pm 0.05\,(\text{stat}) \pm 0.06\,(\text{syst})$ | $5.67^{+0.11}_{-0.11}$ |
| $R_{W/Z}$ | e | $13.62 \pm 0.14\,(\text{stat}) \pm 0.25\,(\text{syst})$ | $13.74^{+0.26}_{-0.25}$ |
| | $\mu$ | $13.00 \pm 0.10\,(\text{stat}) \pm 0.14\,(\text{syst})$ | $13.10^{+0.24}_{-0.23}$ |

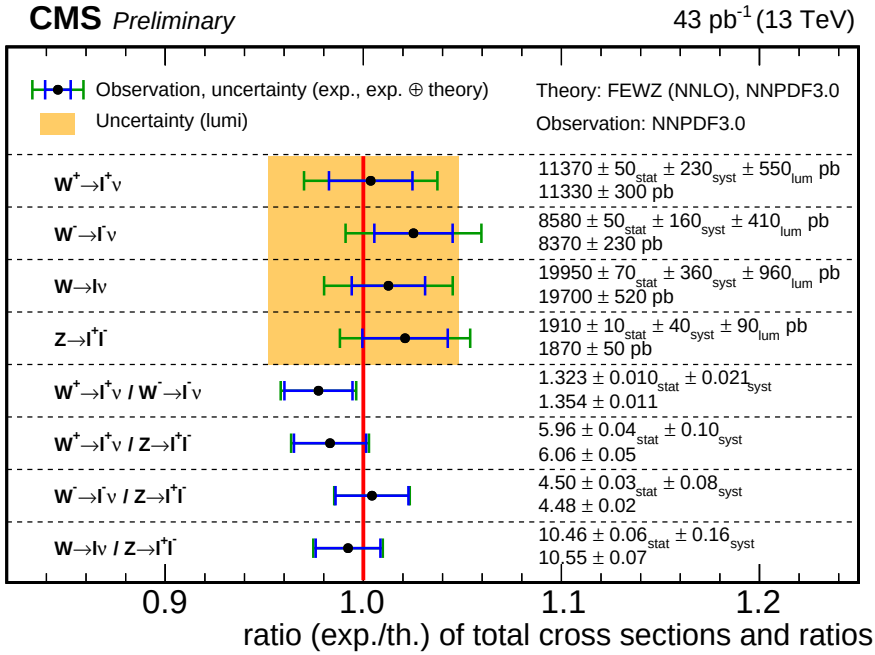


Figure 4: Summary of total inclusive $W^+$, $W^-$, W, and Z production cross sections times branching fractions, W to Z and $W^+$ to $W^-$ ratios, and their theoretical predictions. The shaded box indicates the uncertainties in the luminosity measurement. The inner error bars represent the experimental uncertainties, while outer error bars also include the uncertainties in the theoretical predictions. The individual measurements and theoretical predictions are given numerically on the right.

Table 6: Summary of predicted total inclusive cross sections and their ratios. The predictions were calculated with FEWZ. The PDF uncertainty and scale uncertainty are given for each prediction.

| | NNPDF3.0 | CT14 | MMHT2014 | ABM12LHC | HERAPDF15 |
|---|---|---|---|---|---|
| $\sigma^{tot}_{W^+}$ [pb] | $11330^{+320}_{-270}$ | $11500^{+330}_{-310}$ | $11580^{+260}_{-210}$ | $11730^{+150}_{-130}$ | $11780^{+570}_{-250}$ |
| $\sigma^{tot}_{W^-}$ [pb] | $8370^{+240}_{-210}$ | $8520^{+230}_{-240}$ | $8590^{+190}_{-170}$ | $8550^{+110}_{-90}$ | $8700^{+400}_{-170}$ |
| $\sigma^{tot}_{W}$ [pb] | $19700^{+560}_{-470}$ | $20020^{+560}_{-550}$ | $20170^{+430}_{-390}$ | $20280^{+260}_{-220}$ | $20480^{+960}_{-410}$ |
| $\sigma^{tot}_{Z}$ [pb] | $1870^{+50}_{-40}$ | $1900^{+50}_{-50}$ | $1920^{+40}_{-40}$ | $1920^{+20}_{-20}$ | $1930^{+90}_{-40}$ |
| $\sigma^{tot}_{W^+}/\sigma^{tot}_{W^-}$ | $1.354^{+0.011}_{-0.012}$ | $1.350^{+0.014}_{-0.014}$ | $1.348^{+0.011}_{-0.008}$ | $1.371^{+0.003}_{-0.004}$ | $1.353^{+0.014}_{-0.013}$ |
| $\sigma^{tot}_{W^+}/\sigma^{tot}_{Z}$ | $6.06^{+0.04}_{-0.05}$ | $6.06^{+0.06}_{-0.06}$ | $6.04^{+0.05}_{-0.05}$ | $6.11^{+0.02}_{-0.01}$ | $6.10^{+0.06}_{-0.06}$ |
| $\sigma^{tot}_{W^-}/\sigma^{tot}_{Z}$ | $4.48^{+0.03}_{-0.02}$ | $4.49^{+0.03}_{-0.03}$ | $4.48^{+0.03}_{-0.04}$ | $4.46^{+0.02}_{-0.01}$ | $4.51^{+0.04}_{-0.03}$ |
| $\sigma^{tot}_{W}/\sigma^{tot}_{Z}$ | $10.55^{+0.07}_{-0.06}$ | $10.55^{+0.09}_{-0.09}$ | $10.53^{+0.08}_{-0.09}$ | $10.56^{+0.04}_{-0.02}$ | $10.61^{+0.11}_{-0.09}$ |

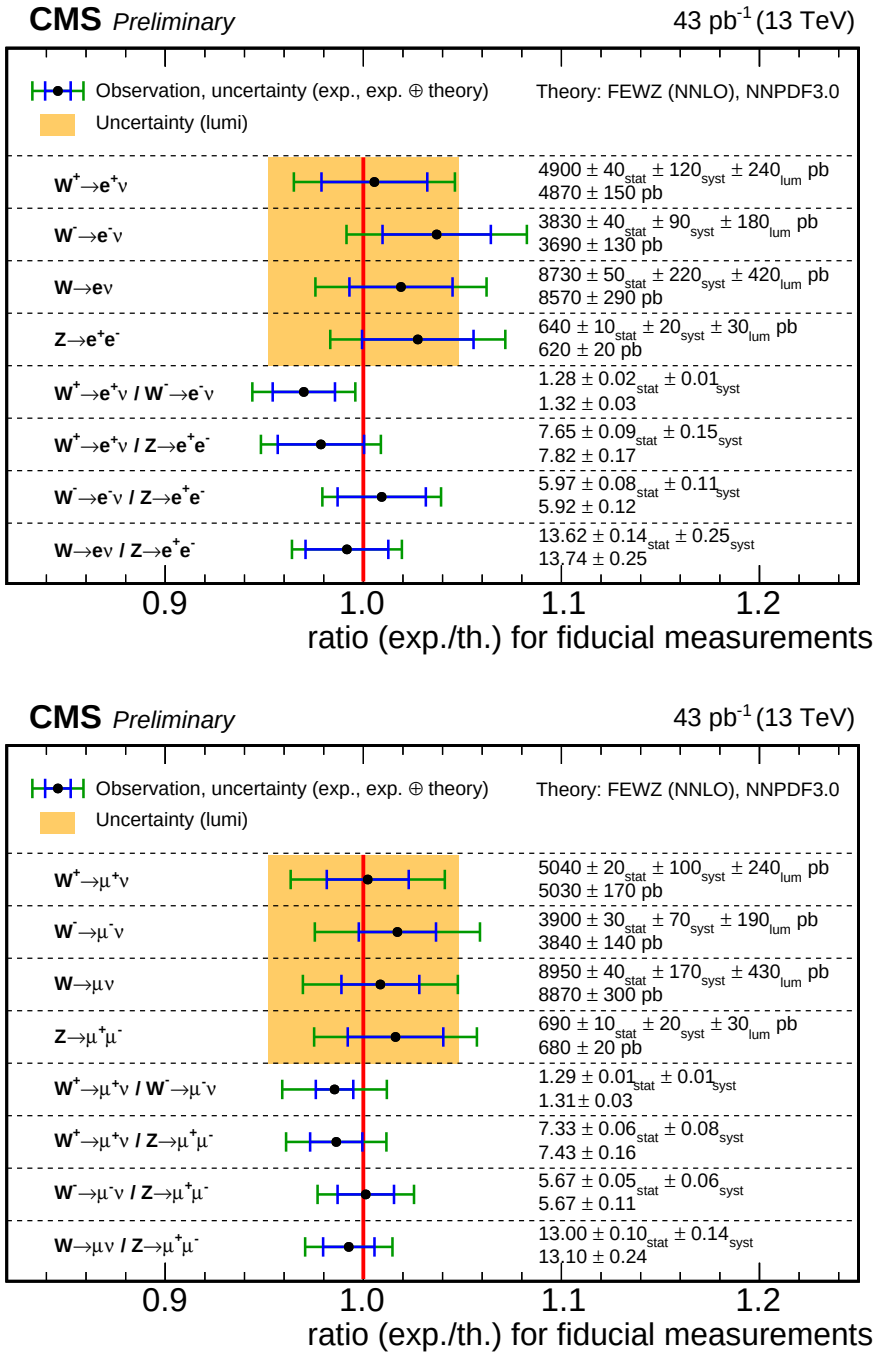


Figure 5: Summary of fiducial inclusive $W^+$, $W^-$, W, and Z production cross sections times branching fractions, W to Z and $W^+$ to $W^-$ ratios, and their theoretical predictions for the electron and muon channel. The shaded box indicates the uncertainties in the luminosity measurement. The inner error bars represent the experimental uncertainties, while outer error bars also include the uncertainties in the theoretical predictions. The individual measurements and theoretical predictions are given numerically on the right.

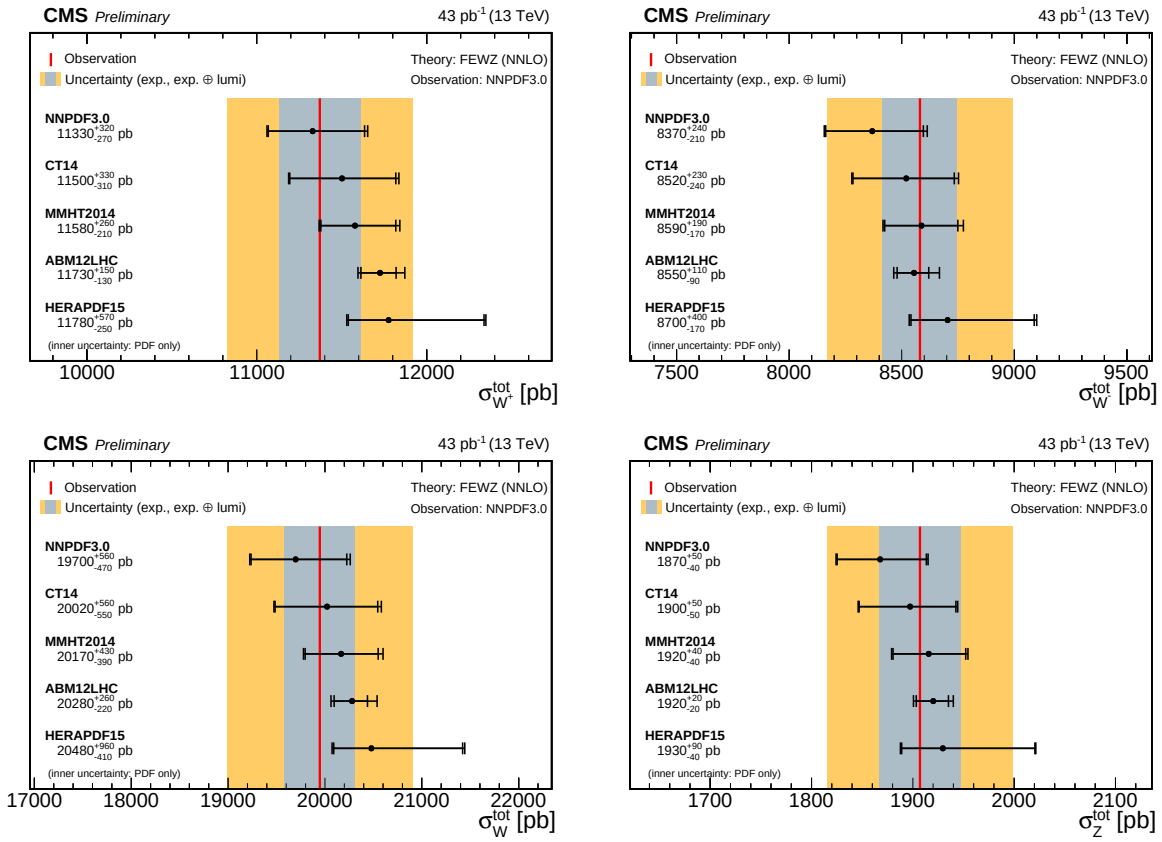


Figure 6: Comparison of measured total inclusive cross sections with predictions for five PDF sets: NNPDF3.0, CT14, MMHT2014, ABM12LHC, and HERAPDF15. The $W^+$(top left), $W^-$ (top right), W (bottom left), and Z (bottom right) total inclusive cross sections are shown.

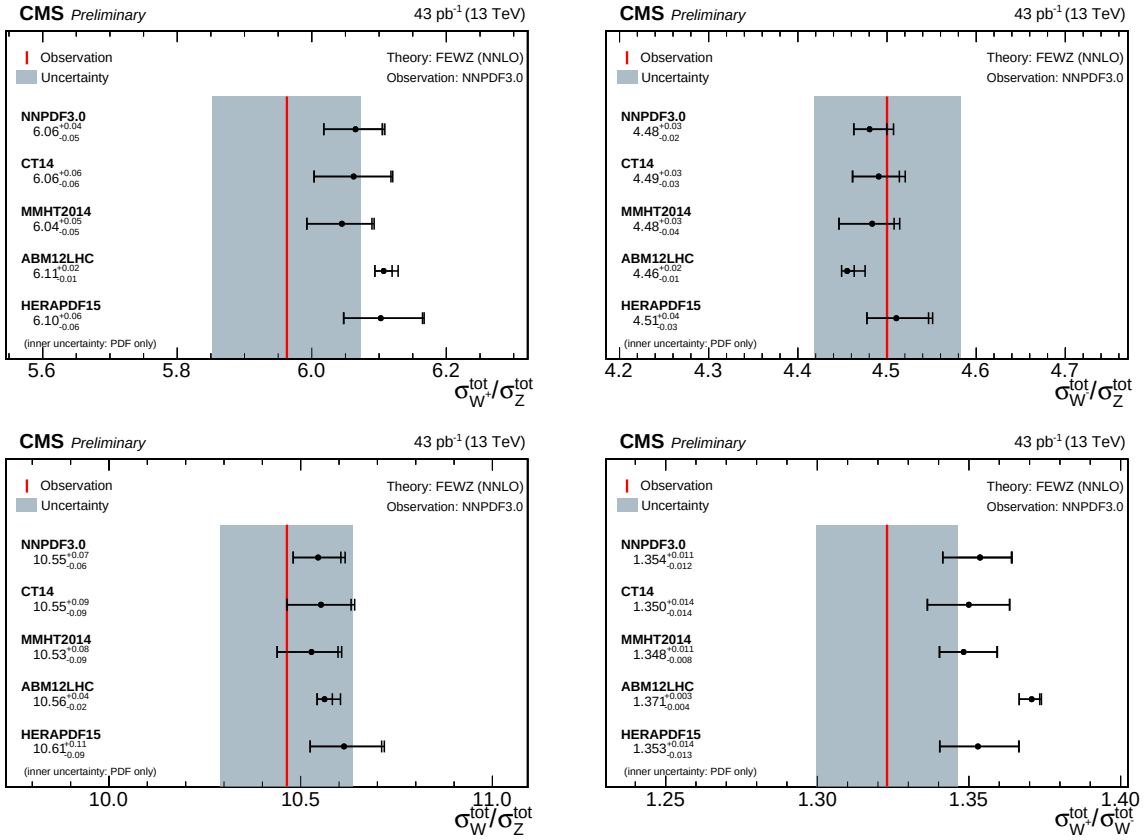


Figure 7: Comparison of measured total inclusive cross section ratios with predictions for five PDF sets: NNPDF3.0, CT14, MMHT2014, ABM12LHC, and HERAPDF15. Ratios of $W^+$(top left) and $W^-$ (top right), and W (bottom left) to Z and $W^+$ to $W^-$ (bottom right) total inclusive cross sections are shown.

times branching fractions versus center-of-mass energy for CMS and experiments at lower-energy colliders [49–54]. The predicted increase of the cross sections with center-of-mass energy is confirmed by the measurements.

# 9 Summary

In summary, a measurement of total inclusive and fiducial W and Z boson production cross sections in pp collisions at $\sqrt{s} = 13\,\text{TeV}$ is presented. Electron and muon final states are studied in a data sample collected with the CMS detector corresponding to an integrated luminosity of up to $43 \pm 2\,\text{pb}^{-1}$. The measured total inclusive cross sections times branching fractions are $\sigma(\text{pp} \to \text{W}^+X) \times \mathcal{B}(\text{W}^+ \to \ell^+\nu) = 11370 \pm 50\,(\text{stat}) \pm 230\,(\text{syst}) \pm 550\,(\text{lumi})\,\text{pb}$, $\sigma(\text{pp} \to \text{W}^-X) \times \mathcal{B}(\text{W}^- \to \ell^-\overline{\nu}) = 8580 \pm 50\,(\text{stat}) \pm 160\,(\text{syst}) \pm 410\,(\text{lumi})\,\text{pb}$, and $\sigma(\text{pp} \to \text{Z}X) \times \mathcal{B}(\text{Z} \to \ell^+\ell^-) = 1910 \pm 10\,(\text{stat}) \pm 40\,(\text{syst}) \pm 90\,(\text{lumi})\,\text{pb}$ for the dilepton mass in the range of 60 to 120 GeV. The measured values agree with next-to-next-to-leading-order QCD cross section calculations. Inclusive cross sections and ratios of cross sections are reported.

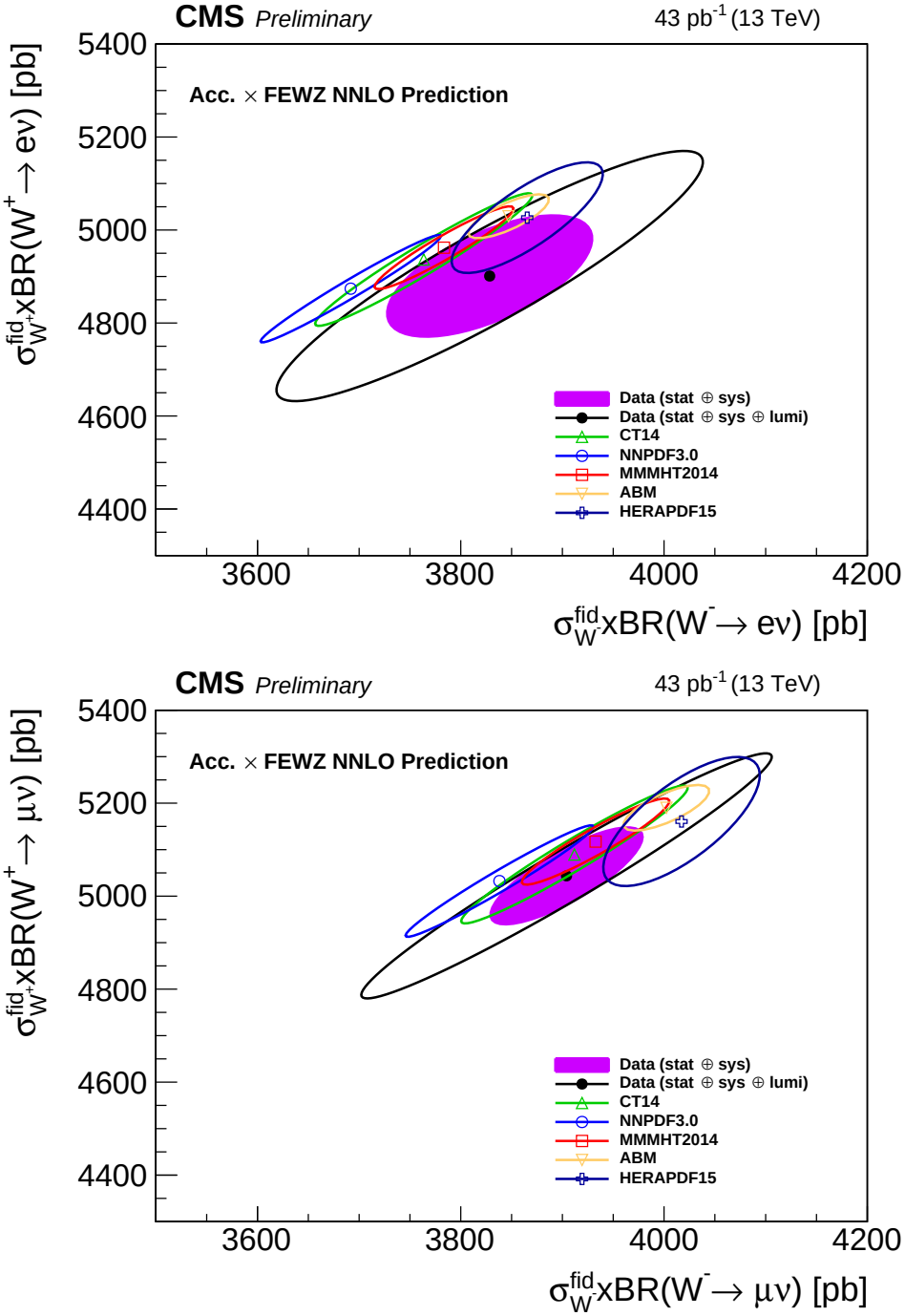


Figure 8: Measured and predicted $W^-$ versus $W^+$ fiducial inclusive production cross sections times branching fractions. The ellipses illustrate the 68% CL coverage for total uncertainties (open) and excluding the luminosity uncertainty (filled). The plots show results for the electron channel (top) and the muon channel (bottom). The uncertainties in the theoretical predictions correspond to the PDF uncertainty components only and are evaluated for five PDF sets: NNPDF3.0, CT14, MMHT2014, ABM12LHC, and HERAPDF15.

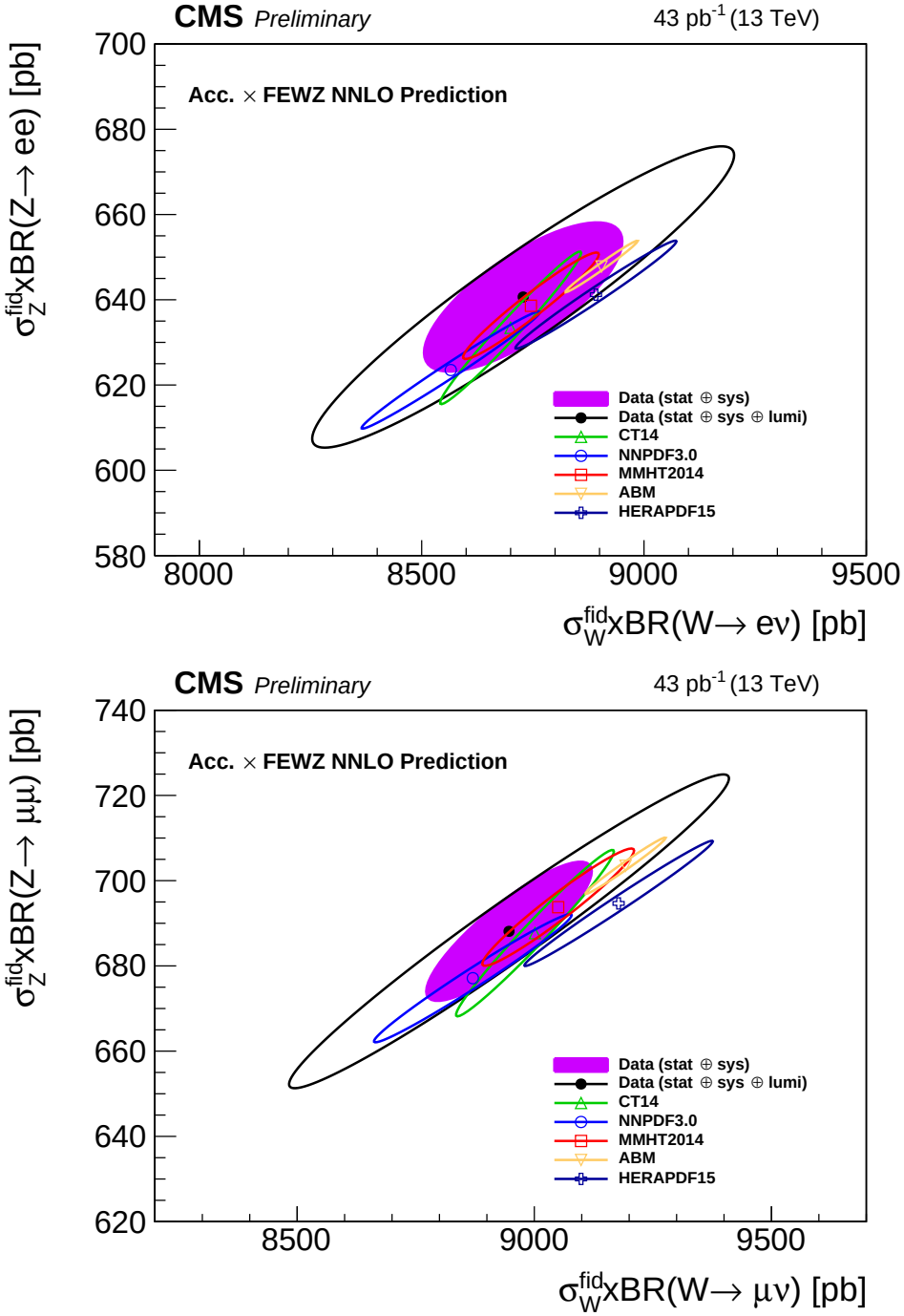


Figure 9: Measured and predicted W versus Z boson fiducial inclusive production cross sections times branching fractions. The ellipses illustrate the 68% CL coverage for total uncertainties (open) and excluding the luminosity uncertainty (filled). The plots show results for the electron channel (top) and muon channel (bottom). The uncertainties in the theoretical predictions correspond to the PDF uncertainty components only and are evaluated for five PDF sets: NNPDF3.0, CT14, MMHT2014, ABM12LHC, and HERAPDF15.

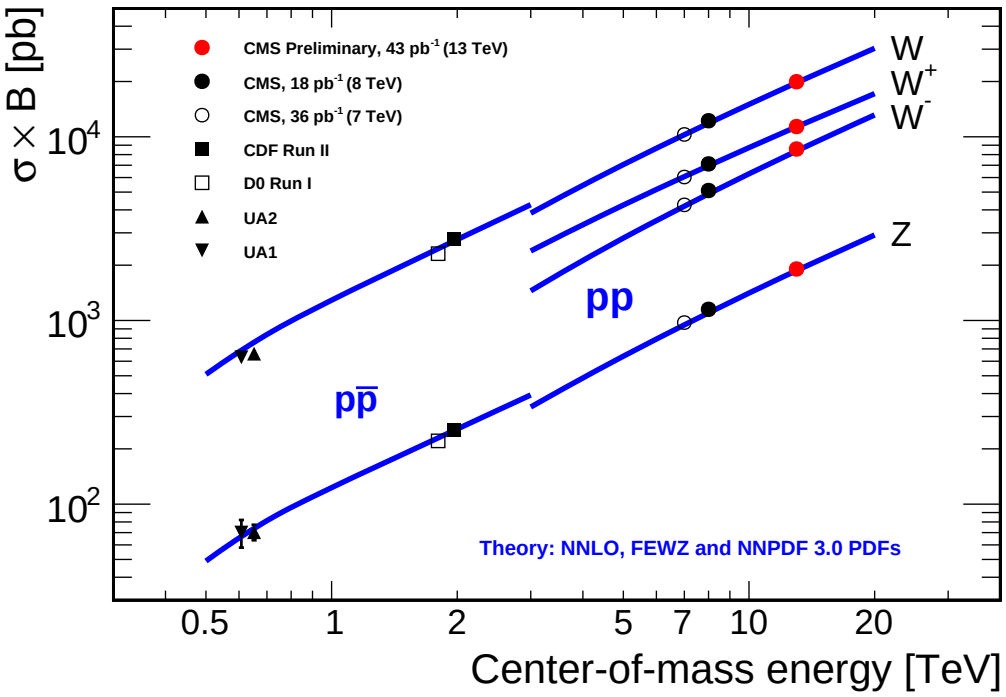


Figure 10: Measurements of the total $W^+$, $W^-$, W, and Z production cross sections times branching fractions versus center-of-mass energy for CMS and experiments at lower-energy colliders. The predicted increase of the cross sections with center-of-mass energy is confirmed by our measurements.

## References


[1] S. D. Drell and T.-M. Yan, "Massive Lepton-Pair Production in Hadron-Hadron Collisions at High Energies", *Phys. Rev. Lett.* **25** (1970) 316, doi:10.1103/PhysRevLett.25.316.

[2] P. J. Rijken and W. L. van Neerven, "Order $\alpha_s^2$ contributions to the Drell-Yan cross section at fixed target energies", *Phys. Rev. D* **51** (1995) 44, doi:10.1103/PhysRevD.51.44.

[3] R. Hamberg, W. L. van Neerven, and T. Matsuura, "A complete calculation of the order $\alpha_s^2$ correction to the Drell-Yan K-factor", *Nucl. Phys. B* **359** (1991) 343, doi:10.1016/0550-3213(91)90064-5.

[4] W. L. van Neerven and E. B. Zijlstra, "The $O(\alpha_s^2)$ corrected Drell-Yan K-factor in the DIS and $\overline{\text{MS}}$ schemes", *Nucl. Phys. B* **382** (1992) 11, doi:10.1016/0550-3213(92)90078-P.

[5] R. V. Harlander and W. B. Kilgore, "Next-to-Next-to-Leading Order Higgs Production at Hadron Colliders", *Phys. Rev. Lett.* **88** (2002) 201801, doi:10.1103/PhysRevLett.88.201801.

[6] C. Anastasiou, L. Dixon, K. Melnikov, and F. Petriello, "High-precision QCD at hadron colliders: Electroweak gauge boson rapidity distributions at next-to-next-to-leading order", *Phys. Rev. D* **69** (2004) 094008, doi:10.1103/PhysRevD.69.094008.

[7] C. M. Carloni Calame, G. Montagna, O. Nicrosini, and A. Vicini, "Precision electroweak calculation of the production of a high transverse-momentum lepton pair at hadron colliders", *J. High Energy Phys.* **10** (2007) 109, doi:10.1088/1126-6708/2007/10/109.

[8] C. M. Carloni Calame, G. Montagna, O. Nicrosini, and A. Vicini, "Precision electroweak calculation of the charged current Drell–Yan process", *J. High Energy Phys.* **12** (2006) 16, doi:10.1088/1126-6708/2006/12/016.

[9] C. M. Carloni Calame, G. Montagna, O. Nicrosini, and M. Treccani, "Multiple photon corrections to the neutral-current Drell-Yan process", *J. High Energy Phys.* **05** (2005) 019, doi:10.1088/1126-6708/2005/05/019.

[10] C. M. Carloni Calame, G. Montagna, O. Nicrosini, and M. Treccani, "Higher-order QED corrections to $W$-boson mass determination at hadron colliders", *Phys. Rev. D* **69** (2004) 037301, doi:10.1103/PhysRevD.69.037301.

[11] CMS Collaboration, "Measurement of the inclusive W and Z production cross sections in pp collisions at $\sqrt{s} = 7$ TeV with the CMS experiment", *J. High Energy Phys.* **10** (2011) 132, doi:10.1007/JHEP10(2011)132.

[12] CMS Collaboration, "Measurement of the inclusive Z cross section via decays to tau pairs in pp collisions at $\sqrt{s} = 7$ TeV", *J. High Energy Phys.* **08** (2011) 117, doi:10.1007/JHEP08(2011)117.

[13] ATLAS Collaboration, "Measurement of the inclusive $W^{\pm}$ and $Z/\gamma*$ cross sections in the $e$ and $\mu$ decay channels in $pp$ collisions $\sqrt{s} = 7$ TeV with the ATLAS detector", *Phys. Rev. D* **85** (2012) 072004, doi:10.1103/PhysRevD.85.072004.

[14] CMS Collaboration, "The CMS experiment at the CERN LHC", *JINST* **3** (2008) S08004, doi:10.1088/1748-0221/3/08/S08004.

[15] J. Alwall et al., "The automated computation of tree-level and next-to-leading order differential cross sections, and their matching to parton shower simulations", *JHEP* **07** (2014) 079, doi:10.1007/JHEP07(2014)079, arXiv:1405.0301.

[16] NNPDF Collaboration, "Parton distributions for the LHC Run II", *JHEP* **04** (2015) 040, doi:10.1007/JHEP04(2015)040, arXiv:1410.8849.

[17] T. Sjostrand, S. Mrenna, and P. Z. Skands, "PYTHIA 6.4 Physics and Manual", *JHEP* **05** (2006) 026, doi:10.1088/1126-6708/2006/05/026, arXiv:hep-ph/0603175.

[18] T. Sjstrand et al., "An Introduction to PYTHIA 8.2", *Comput. Phys. Commun.* **191** (2015) 159–177, doi:10.1016/j.cpc.2015.01.024, arXiv:1410.3012.

[19] S. Alioli, P. Nason, C. Oleari, and E. Re, "NLO Vector Boson Production Matched with Shower in POWHEG", *J. High Energy Phys.* **07** (2008) 060, doi:10.1088/1126-6708/2008/07/060.

[20] P. Nason, "A New Method for Combining NLO QCD with Shower Monte Carlo Algorithms", *J. High Energy Phys.* **11** (2004) 040, doi:10.1088/1126-6708/2004/11/040.

[21] S. Frixione, P. Nason, C. Oleari, "Matching NLO QCD computations with parton shower simulations: the POWHEG method", *J. High Energy Phys.* **11** (2007) 070, doi:10.1088/1126-6708/2007/11/070.

[22] S. Alioli, P. Nason, C. Oleari, and E. Re, "A General Framework for Implementing NLO Calculations in Shower Monte Carlo Programs: the POWHEG BOX", *J. High Energy Phys.* **06** (2010) 043, doi:10.1007/JHEP06(2010)043.

[23] GEANT4 Collaboration, "GEANT4 – a simulation toolkit", *Nucl. Instrum. Meth. A* **506** (2003) 250, doi:10.1016/S0168-9002(03)01368-8.

[24] W. Adam, R. Frühwirth, A. Strandlie, and T. Todor, "Reconstruction of Electrons with the Gaussian-Sum Filter in the CMS Tracker at the LHC", Technical Report CMS-NOTE-2005-001, 2005.

[25] CMS Collaboration, "CMS tracking performance results from early LHC operation", *Eur. Phys. J. C* **70** (2010) 1165, doi:10.1140/epjc/s10052-010-1491-3.

[26] CMS Collaboration, "Energy calibration and resolution of the CMS electromagnetic calorimeter in pp collisions at $\sqrt{s}$ = 7 TeV", *JINST* **8** (2013) P09009, doi:10.1088/1748-0221/8/09/P09009, arXiv:1306.2016.

[27] CMS Collaboration, "Measurement of the Isolated Prompt Photon Production Cross Section in pp Collisions at $\sqrt{s} = 7$ TeV", *Phys. Rev. Lett.* **106** (2011) 082001, doi:10.1103/PhysRevLett.106.082001.

[28] S. Baffioni et al., "Electron reconstruction in CMS", *Eur. Phys. J. C* **49** (2007) 1099, doi:10.1140/epjc/s10052-006-0175-5.

[29] CMS Collaboration, "Commissioning of the Particle-flow Event Reconstruction with the first LHC collisions recorded in the CMS detector", CMS Physics Analysis Summary CMS-PAS-PFT-10-001, 2010.

[30] CMS Collaboration, "Commissioning of the particle-flow event reconstruction with leptons from J/Ψ and W decays at 7 TeV", CMS Physics Analysis Summary CMS-PAS-PFT-10-003, 2010.

[31] CMS Collaboration, "Performance of muon identification in pp collisions at $\sqrt{s}$ = 7 TeV", CMS Physics Analysis Summary CMS-PAS-MUO-10-002, 2010.

[32] CMS Collaboration, "Performance of CMS muon reconstruction in cosmic-ray events", *JINST* **5** (2010) T03022, doi:10.1088/1748-0221/5/03/T03022.

[33] C. Balázs and C.-P. Yuan, "Soft gluon effects on lepton pairs at hadron colliders", *Phys. Rev. D* **56** (1997) 5558, doi:10.1103/PhysRevD.56.5558.

[34] E. Barberio, B. van Eijk, and Z. Wąs, "Photos — a universal Monte Carlo for QED radiative corrections in decays", *Comp. Phys. Commun.* **66** (1991) 115, doi:10.1016/0010-4655(91)90012-A.

[35] D. Bertolini, P. Harris, M. Low, and N. Tran, "Pileup Per Particle Identification", *JHEP* **10** (2014) 59, doi:10.1007/JHEP10(2014)059, arXiv:1407.6013.

[36] J. M. Campbell and R. K. Ellis, "MCFM for the Tevatron and the LHC", *Nucl. Phys. Proc. Suppl.* **205** (2010) 10, doi:10.1016/j.nuclphysbps.2010.08.011, arXiv:1007.3492.

[37] S. van der Meer, "Calibration of the effective beam height in the ISR", Technical Report CERN-ISR-PO-68-31. ISR-PO-68-31, 1968.

[38] K. Melnikov and F. Petriello, "$W$ Boson Production Cross Section at the Large Hadron Collider with $\mathcal{O}(\alpha^2)$ Corrections", *Phys. Rev. Lett.* **96** (2006) 231803, doi:10.1103/PhysRevLett.96.231803.

[39] R. Gavin, Y. Li, F. Petriello, and S. Quackenbush, "FEWZ 2.0: A code for hadronic Z production at next-to-next-to-leading order", *Comput. Phys. Commun.* **182** (2011) 2388–2403, doi:10.1016/j.cpc.2011.06.008, arXiv:1011.3540.

[40] R. Gavin, Y. Li, F. Petriello, and S. Quackenbush, "W Physics at the LHC with FEWZ 2.1", *Comput. Phys. Commun.* **184** (2013) 208–214, doi:10.1016/j.cpc.2012.09.005, arXiv:1201.5896.

[41] Y. Li and F. Petriello, "Combining QCD and electroweak corrections to dilepton production in FEWZ", *Phys. Rev.* **D86** (2012) 094034, doi:10.1103/PhysRevD.86.094034, arXiv:1208.5967.

[42] A. Martin, W. Stirling, R. Thorne, and G. Watt, "Uncertainties on $\alpha_s$ in global PDF analyses and implications for predicted hadronic cross sections", *Eur. Phys. J. C* **64** (2009) 653, doi:10.1140/epjc/s10052-009-1164-2.

[43] G. Watt, "Parton distribution function dependence of benchmark Standard Model total cross sections at the 7 TeV LHC", *J. High Energy Phys.* **09** (2011) 069, doi:10.1007/JHEP09(2011)069.

[44] A. Martin, W. Stirling, R. Thorne, and G. Watt, "Heavy-quark mass dependence in global PDF analyses and 3- and 4-flavour parton distributions", *Eur. Phys. J. C* **70** (2010) 51, doi:10.1140/epjc/s10052-010-1462-8.

[45] S. Dulat et al., "The CT14 Global Analysis of Quantum Chromodynamics", arXiv:1506.07443.

[46] L. A. Harland-Lang, A. D. Martin, P. Motylinski, and R. S. Thorne, "Parton distributions in the LHC era: MMHT 2014 PDFs", *Eur. Phys. J.* **C75** (2015), no. 5, 204, doi:10.1140/epjc/s10052-015-3397-6, arXiv:1412.3989.

[47] S. Alekhin, J. Blumlein, and S. Moch, "The ABM parton distributions tuned to LHC data", *Phys. Rev.* **D89** (2014), no. 5, 054028, doi:10.1103/PhysRevD.89.054028, arXiv:1310.3059.

[48] H1 and ZEUS Collaboration, "Combined Measurement and QCD Analysis of the Inclusive ep Scattering Cross Sections at HERA", *J. High Energy Phys.* **01** (2010) 109, doi:10.1007/JHEP01(2010)109.

[49] UA1 Collaboration, "Intermediate Vector Boson Cross-sections at the CERN Super Proton Synchrotron Collider and the Number of Neutrino Types", *Phys. Lett. B* **198** (1987) 271, doi:10.1016/0370-2693(87)91510-3.

[50] UA2 Collaboration, "A Measurement of the W and Z Production Cross-sections and a Determination of $\Gamma_W$ at the CERN $\overline{p}p$ collider", *Phys. Lett. B* **276** (1992) 365, doi:10.1016/0370-2693(92)90333-Y.

[51] CDF Collaboration, "Measurement of $\sigma \times B(W \to e\nu)$ and $\sigma \times B(Z \to e^+e-)$ in $p\overline{p}$ collisions at $\sqrt{s} = 1.8$ TeV ", *Phys. Rev. Lett.* **76** (1996) 3070, doi:10.1103/PhysRevLett.76.3070.

[52] CDF Collaboration, "Measurement of $Z^0$ and Drell-Yan production cross section using dimuons in $\overline{p}p$ collisions at $\sqrt{s} = 1.8$ TeV ", *Phys. Rev. D* **59** (1999) 052002, doi:10.1103/PhysRevD.59.052002.

[53] CDF Collaboration, "Measurements of Inclusive W and Z Cross-sections in $p\overline{p}$ Collisions at $\sqrt{s} = 1.96$ TeV ", *J. Phys. G* **34** (2007) 2457, doi:10.1088/0954-3899/34/12/001.

[54] D0 Collaboration, "Extraction of the width of the W boson from measurements of $\sigma(p\overline{p} \to W + X) \times B(W \to e\nu)$ and $\sigma(p\overline{p} \to Z + X) \times B(Z \to ee)$ and their ratio", *Phys. Rev. D* **61** (2000) 072001, doi:10.1103/PhysRevD.61.072001.